Routes to visible light active C-doped TiO_2 photocatalysts using carbon atoms from the Ti precursors.

James A. Sullivan[a*], Elaine M. Neville[a], Rory Herron[a], K Ravinandrathan Thampi[b*], J.M. Donal MacElroy[b].

[a] SFI Strategic Research Cluster in Solar Energy Conversion, UCD School of Chemistry and Chemical Biology, UCD Science Centre, University College Dublin, Belfield, Dublin 4, Ireland

[b] SFI Strategic Research Cluster in Solar Energy Conversion, UCD School of Chemical and Bioprocess Engineering, University College Dublin, Belfield, Dublin 4, Ireland

1.0 Abstract

In this work, different thermal treatments of titanium isopropoxide-derived photo-catalyst precursors, designed with the purpose of generating C-doped TiO_2 photo-catalysts using carbon atoms present in the TiOx gel precursors as dopants, are presented. Specifically, these look at varying the standard calcination techniques using heat treatments in He (rather than calcination in air) and lower temperature calcinations (200 °C rather than 500 °C). The formed materials are characterised using N_2 physisorption, XRD, UV Visible spectroscopy and XPS and their activities in promoting the oxidation of 4-chlorophenol under visible-light-only conditions were analysed. The nature of carbon remaining on the (or in the) material is discussed found to be both surface graphitic carbon and carbon present in anionic dopant positions. The different contributions of each type of carbon to the catalytic photo-activity under visible light are discussed.

Keywords: C-doped TiO_2, catalyst preparation, photocatalysis.

2.0 Introduction

Photo-generated electron hole pairs in TiO_2 are effective redox mediators for a range of process including H_2 generation from water splitting [1, 2], photo-reforming of organic materials to H_2 and CO_2 [3, 4] and the oxidation of a range of aqueous phase organic pollutant materials [5-10].

Regarding the latter application, the mechanism of pollutant oxidation involves several processes that are both surface mediated, where direct oxidation (hole neutralisation by removal of electrons from adsorbed organic species) and direct reduction (electron transfer from catalyst conduction band to adsorbed species) reactions happen on the photo catalyst surface, and solution mediated (where oxidants formed on the photo-catalysts subsequently carry out homogeneous oxidations in solution) [9, 10].

More extensive use of TiO_2 visible-light driven photo-catalysts is curtailed by the relatively large bandgap of the material. In order to promote electrons between the valance and conduction bands (generating redox active electron hole pairs) the energy of light absorbed must be above 3.2 eV (below a wavelength of 387 nm). This restricts the utilizable solar photons (and therefore the efficiency in promoting redox reactions) to those in the UV region of the spectrum, *i.e.* only 4% of the spectrum is useful [11].

Efforts to move absorbance of the materials into the visible region of the spectrum have – for the most part – involved attempts to dope the TiO_2 using either metallic (e.g. W, Cr, Sn *etc.*) [12-15] or non-metallic (*e.g.* C, N) [16-24] elements and these are reported to occupy cationic or anionic sites in the TiO_2 lattice respectively. These dopants decrease the band gap through a combination of adding

electrons in energy levels above the valance band or adding orbitals of energy below the energy of the conduction band.

Carbon doping has been an area of intense research interest and the characterisation of the formed C-TiO_2 photo-catalyst has normally been carried out using a combination of XPS and UV Visible spectroscopy. The latter technique confirms reductions in the band gap while the latter shows the nature of the C-dopant (surface carbonate, substitutional anionic, interstitial *etc*.

In the main, the doping of TiO_2 with C atoms has involved the use of sources of carbon either added to the TiO_2 post preparation or added to a mixture from which TiO_2 condensed or precipitated. In some instances C-doped TiO_2 has been prepared using a sol-gel technique where the dopant carbon atoms arose from a titanium alkoxide precursor which had remained within the lattice following the final TiO_2 preparation [25, 26]. In their work Park *et al.* and Yang *et al.* lowered the calcination temperature of their final material in order to conserve carbon atoms within the final TiO_2 lattice.

In this work we have attempted a systematic study of a range of heat treatments on gels that are derived from condensation of a titanium isopropoxide precursor. These treatments, which involve high temperature treatments in He and low temperature oxidations in O_2 have generated materials which we have characterised using XRD, UV Visible spectroscopy and XPS. We have subsequently applied the synthesised materials in the photo-oxidation of a model pollutant (4-chlorophenol).

3.0 Experimental

3.1 Catalyst synthesis

Dried sol-gel precipitates derived from the hydrolysis of titanium isopropoxide were subjected to different heat and chemical treatments with the aim of (a) crystallizing TiO_2 and (b) retaining C atoms as anionic dopants within the TiO_2 lattice.

To form the first of these materials (designated as C-TiO_2(He)) the following process was used. 30 mL of deionized water in an ice bath was vigorously stirred and 8 mL (0.028 mol) of titanium isopropoxide (97 %, Aldrich) was added dropwise. The mixture was stirred for 12 h and aged for 24 h at room temperature. Water removal was accomplished by drying at 80 °C in air. The sample thus obtained was thoroughly ground with an agate mortar and pestle. The material was then loaded into a pyrex glass tubular reactor and held in place using plugs of quartz wool. 100 mL min^{-1} of He was flowed through the reactor and the temperature was ramped at a rate of 20 °C min^{-1} from room temperature to 500 °C. The material was held at this temperature for 2 h in the He flow. The final material had a surface area of 44 m^2 g^{-1}.

To form a C-TiO_2 (RCT) sample (where RCT refers to a reduced calcination temperature), 30 mmol of Ti isopropoxide (9 mL) was dissolved in 50 mL of isopropanol in an ice bath. 7 mmol of perchloric acid (7 mL of 1 mol/L solution) was added while vigorously stirring. The mixture was left to age for 24 h and the resultant product was dried at 80 °C and ground in an agate mortar and pestle. The material was then placed in a chamber furnace where the temperature was ramped at a rate of 5 °C min^{-1} in air from room temperature up to 200 °C and held at this temperature for 2 h. This material had a surface area of 203 m^2 g^{-1}.

3.2 Material Characterisations.

Thermogravimetric analysis coupled to mass spectrometry of exit gases was carried out using a (TA Instruments, TGA 500 coupled to a Hiden Analytical HPR20-QIC Atmospheric Gas Analysis System. In certain experiments TGA / MS was used to look at the behaviours of the precursors at different temperatures and durations. Powder XRD patterns were collected using a Siemens D500 Kristalloflex using Cu Kα radiation over a 2θ range from 20 ° to 90 °. Diffuse Reflectance UV-Visible spectroscopy (DRS) was carried out using an Analytik Jena Specord 210 spectrometer equipped with an integrating sphere attachment for measurement of spectra from powder samples. N_2 physisorption isotherms were collected on a Quantachrome Nova 2000e. X-ray Photoelectron Spectroscopy (XPS) was carried out with a Kratos AXIS 165 spectrometer using a monochromatic X-ray source (Al Kα 1486.58 eV).

3.3 Photocatalytic oxidation reaction

The photocatalytic activity of the materials was tested by investigating the photocatalytic degradation of 4-chlorophenol solutions in the presence of our photocatalysts under illumination. Typically 80 mg of photocatalyst powder was dispersed in 40 mL of a 0.5 mM solution of 4-chlorophenol. The mixture was sonicated for 15 minutes before being purged with air for 5 minutes. Samples were stirred in the dark for 30 minutes in order to reach an adsorption – desorption equilibrium. Irradiation was carried out in an Atlas Suntest CPS+ solar simulator unit containing a 1500 Watt Air Cooled Xenon Arc Lamp. The solar simulator unit provides a AM 1.5 G spectrum. The solar simulator unit was also used in conjunction with a UV filter film ($\lambda > 410$ nm).

Samples were extracted after 1 h and the degradation of 4-chlorophenol was monitored using Total Organic Carbon (TOC) analysis. This was carried out using a Shimadzu TOC V-CPH. To determine the

TOC content both the Total Carbon (TC) and Inorganic carbon (IC) components were measured, the TOC being the difference between the IC and the TC.

4.0 Results and discussion

4.1 XRD analysis

X-ray diffraction (XRD) analysis was carried out to determine the crystal phase (anatase, rutile *etc.*) composition and crystalline particle sizes of the samples. XRD patterns were obtained from the material prior to any of the different heat treatments (the precursor material), and both of the C-doped samples detailed above. A profile from a sample of TiO_2 prepared by an air oxidation of the precursor in O_2 (at 500 °C) is shown for reference.

Figure 1

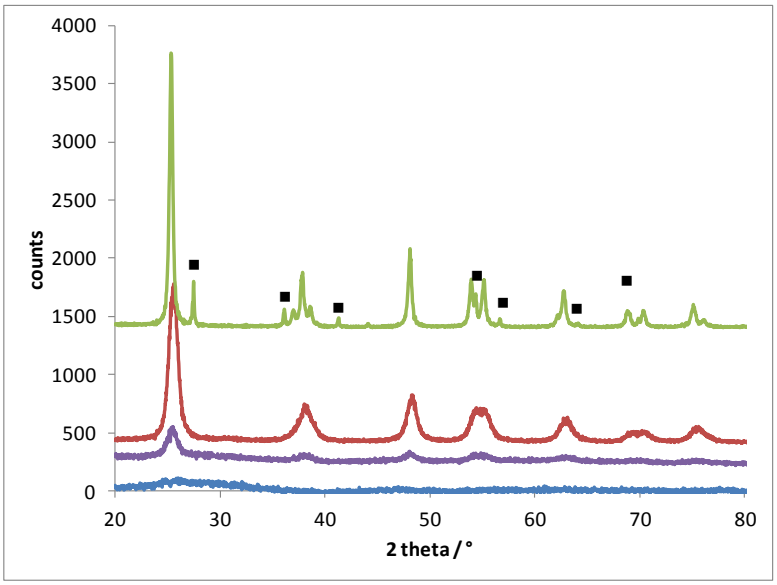

Figure 1: XRD profiles from the TiO_2 precursor prior to calcination (bottom profile), a C-TiO_2(RCT) sample prepared by calcining the precursor at 200 °C for 2 h (second profile), a TiO_2 sample prepared by calcining the precursor at 500 °C for 2h in air (third profile) and a C-TiO_2 (He) sample prepared by treating the precursor in He at 500 °C for 2h. ■ indicates reflections from rutile TiO_2.

XRD analysis of the precursor material revealed no pattern confirming that the material was amorphous. TiO_2 prepared by calcining the precursor in air for 2h at 500 °C showed only anatase phase peaks and the particle size (as measured using the Scherrer equation [27]) was ~ 9 nm.

On the contrary, the material prepared following the He treatment at 500 °C showed both anatase and rutile peaks. Application of the technique of Spurr *et al.* [28] to estimate the phase composition of this mixture gives an anatase rutile ratio of 83:17 and Scherrer analysis gives relatively higher particle sizes of 21 nm (anatase) and 34 nm (rutile).

The catalyst which had been calcined for 200 °C in air for 2 h gave an XRD profile which was indicative of a far less crystalline material with particle sizes determined to be ~ 6 nm. This is not surprising given that higher temperatures are required for crystallization.

What is surprising is that the TiO_2 crystallized in the absence of O_2 had larger particles (and a proportion of rutile) that was not present in the material calcined in air since the anatase → rutile transition is reported to happen above 800 °C and these materials were treated only to 500 °C. Larger crystals (to an extent) are considered to be more useful in photocatalysis as it minimises electron-hole recombinations, although it should be recalled that there is a trade off between these crystal sizes and the available surface area for reactions.

The unit cell parameters of these materials was determined from analysis of these profiles [29] and the sizes of the anatase unit cells were determined to be 135.0453 +/- 0.0082 $Å^3$ for the TiO_2 sample, 135.3058 +/- 0.0187 $Å^3$ for the material calcined at 200 °C and 136.3409 +/- 0.0136 $Å^3$

(anatase) and 62.6271 +/- 0.0109 Å^3 (rutile). Given the latter two of these materials contain the same amounts of doped anionic C atoms (see later) it seems there is no relationship between the unit cell volume and the presence or absence of carbon dopant.

There is also some XRD evidence for the incorporation of C atoms into the lattice of the C-TiO_2 (He) sample in that there was a peak shift for the (101) anatase peak which was at 2Θ = 25.48 for the TiO_2 sample and 2Θ= 25.34 for the C-TiO_2 (He) material. This has been related in literature to distortions in the normal crystal lattice by incorporation of dopants such as carbon or nitrogen [26]. Due to the lack of crystallininty of the material, such a measurement was not possible from the XRD profiles of the C-TiO_2 (RCT) catalysts.

4.2 UV Visible spectroscopy and band gap calculations

The C-TiO_2 (He) sample was grey in colour while the TiO_2 was white and the C-TiO_2 (RCT) was yellow. In general, a yellow colour in a material shows that the material absorbs in the purple part of the visible spectrum. Figure 2 shows the UV-vis spectra of the three studied materials. The TiO_2 sample absorbs small portions of radiation above 400 nm while it is clear that in the case of both nominally C-doped materials the absorbance has been shifted further into the visible region. This is an indication of the incorporation of C atoms into anionic sites within the TiO_2 lattice. There is another difference in that the absorbance of the C-TiO_2 (He) sample extends unchanged through the visible region of the spectrum.. We will further discuss the origin of this absorbance below which – on first viewing may relate to the deposition of a carbonaceous overlayer or to the presence of Ti^{3+} sites within the material (see later).

Figure 2

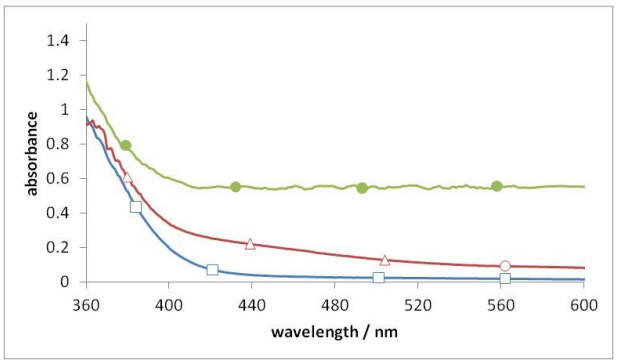

Figure 2. UV Visible absorbance spectra of TiO_2 (□), C-TiO_2 (RCT) (△) and C-TiO_2 (He) (●).

Bandgap estimations can be made for these materials by determining the absorption edge. A tangent is drawn from the slope of the high energy feature and the intercept of this with the absorbance of zero is the onset wavelength and can be used to calculate the bandgap. Using the different absorbance onsets and it was found that the TiO_2 had a bandgap of 3.1 eV while both of the C-TiO_2 samples had smaller bandgaps (estimated at 2.95 eV for C-TiO_2 (He) and 2.90 eV for the C-TiO_2 (RCT) sample. This is further confirmation that C dopants are present in the anionic doping sites of these materials.

In order to further probe the material giving rise to the extended absorbance of the C-TiO_2 (He) sample in the visible region of the spectrum, a series of materials were produced using modifications of the He heat treatment. These involved additions of O_2 into the He treatment streams for varied times and at varied temperatures. The series of materials produced were then analysed using UV Visible spectroscopy and the resultant spectra are shown in figure 3.

Figure 3(a).

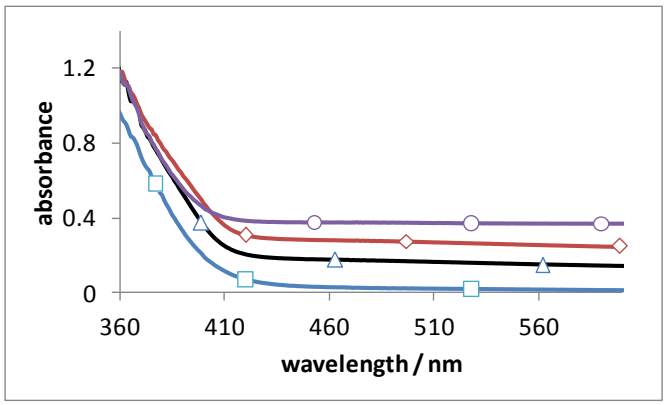

Figure 3(b).

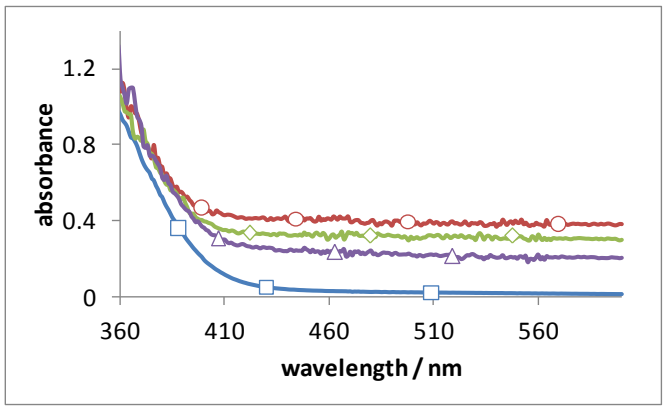

Figure 3(a) shows UV Vis spectra of a series of materials that had been exposed to 20% O_2 for 2 min. at 50 °C (❍), 200 °C (✧ – this is the He-200 material referred to later) and 400 °C (△) during the initial temperature ramp in He (before exposure to He for 2h at 500 °C). Figure 3(b) shows UV Vis spectra of a series of materials that had been exposed to 20% O_2 for 1 (❍), 2 (✧) and 3 minutes (△) at 250 °C during the initial temperature ramp in He. The spectrum of fully oxidised TiO_2 (□) is also shown for reference.

Figure 3 (a) shows the spectra of a series of materials that underwent oxidation for 2 minutes at different temperatures (50 °C, 200 °C and 400 °C) throughout the ramp in He, *i.e.* the ramp was held at these temperatures for 2 minutes, He was replaced with 20% O_2 in He for this time, and then the O_2 was removed and the ramp to 500 °C in He recommenced.

For all materials the band gaps remain the same at ~ 2.90 eV, but in each case it can also be seen that for each the flat feature extending from 410 nm through the visible part of the spectrum decreases in intensity as progressively harsher oxidation treatments are used. This indicates that the material that gives rise to this flat extended absorbance in the visible region of the spectrum relates to a species which is removed by oxidation. Furthermore it seems that these oxidation treatments do not result in the removal of any dopant C (consider the unchanging bandgaps).

There are two possible species that might lead to this absorbance, viz. graphitic C(s) that remains on the surface of the material following the treatment in He or alternately Ti^{3+} species that were generated following O removal from the TiO_2 lattice during the high temperature treatment in He. The concentrations of both of these species would decrease following more severe oxidation treatments – so this technique is not particularly useful in discriminating between them.

4.3 Temperature programmed oxidation and thermo-gravimetric analysis.

A temperature programmed oxidation experiment (in combination with TGA) was carried out to further characterise the material that led to this enhanced absorbance and the results of this experiment are shown in figure 4. The evolved CO_2 profile (figure 4(a)) begins to form at temperatures above 600 °C (indicative of graphitic carbon combustion [30]). The concentration of CO_2 measured increased throughout the remainder of the temperature ramp before the experiment was stopped at 1000 °C. The associated TGA (figure 4 (b)) shows a lower temperature mass loss which is associated with dehydration, and a continuous mass loss at temperatures above 600 °C which relates to the removal of C(s) from the surface.

Figure 4(a)

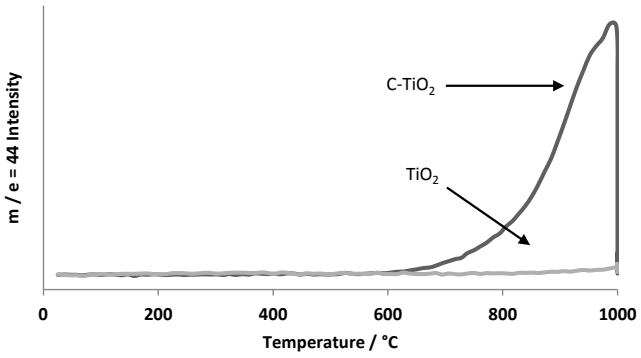

Figure 4(b)

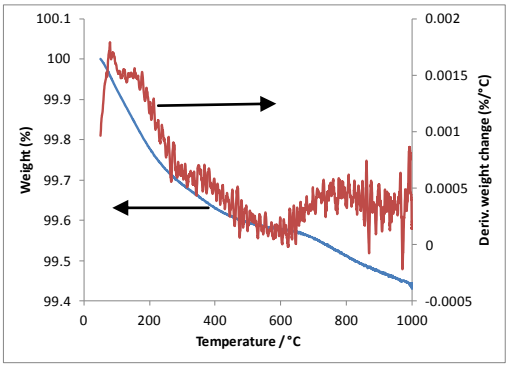

Figure 4(a) CO_2 production from a temperature programmed oxidation of the C-TiO_2 (He) catalyst (upper profile) and TiO_2 (lower profile) (b) concomitant TGA experiment showing mass and differential mass profiles from the C-TiO_2 (He) catalyst .

Attempts to relate the mass loss to doped C are fraught since removal of C(s) – which most of this carbon presumably is – should result in a decrease in the mass of the sample, but removal of anionic dopant C should result in a (smaller) increase in mass (as C atoms are replaced by O atoms in the lattice).

Figure 5 shows the analogous TGA and TPO profiles collected from the C-TiO_2 (RCT) material. It is clear that a significant amount of combustible organic material is removed from this catalyst during the TGA experiment. The temperatures at which these are removed suggest the material is hydro-carbonaceous rather than graphitic in nature. Most of the carbon is removed by a temperature of 450 °C although there does seem to be a small graphitic feature at a temperature of ~650 °C visible in the TPO profile.

Figure 5(a) **Figure 5(b)**

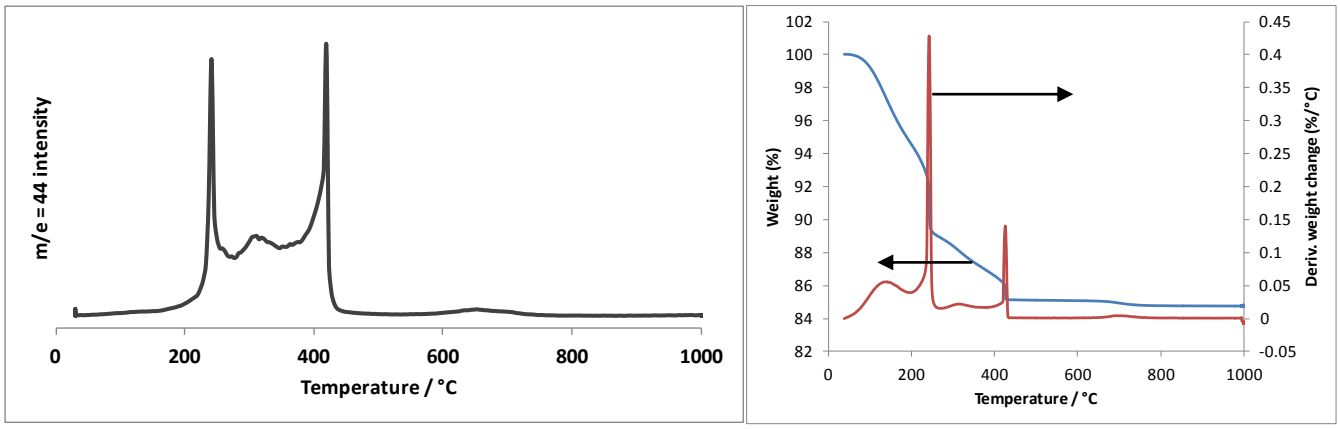

Figure 5(a) CO_2 production from a temperature programmed oxidation of the C-TiO_2 (RCT) catalyst (b) concomitant TGA experiment showing mass and differential mass profiles from the same catalyst.

4.3 XPS analysis

The evidence for doping presented above involves a shifted XRD profile (in the case of the C-TiO_2 (He) catalyst) and lowered bandgaps (as measured using UV visible spectroscopy) in the case of both doped catalysts. For direct evidence of anionic doping, XPS is employed. Looking at C in XPS is also a fraught operation due to the presence of adventitious C atoms within the XPS chamber as well as issues associated with peaks relating to surface carbonate on the catalyst masking those related to the Ti-C species where the C atom is present as an anionic dopant. The latter case is defined by a peak in the XPS spectrum at 282 eV. We have previously noted [24, 31, 32] that sputtering the sample in a high energy beam of Ar ions can etch away the catalyst surface and expose sub-surface layers. In so doing, the sputtering also removes the surface carbonate and its peaks are removed from subsequent XPS spectra. The peak at 285 eV is an instrumental artefact related to adventitious C and is present in all XPS spectra.

Figure 6

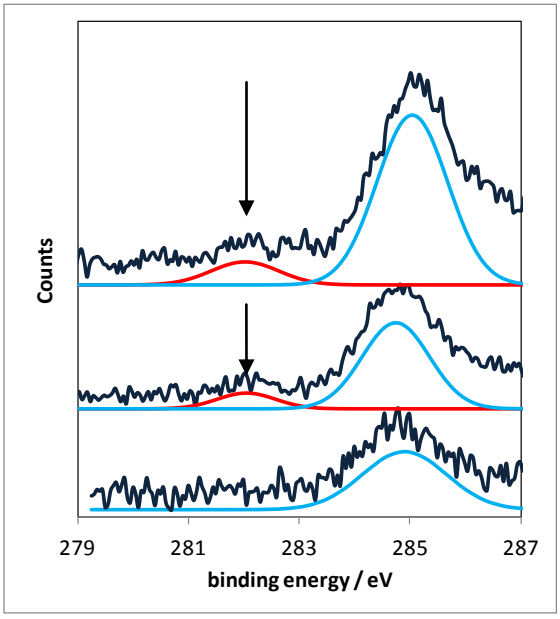

Figure 6. Displaced XPS spectra (C 1s region) of C-TiO_2 (RCT) (top profile), C-TiO_2 (He) (middle profile) and TiO_2 (lower profile). The samples were sputtered for 8 min with low energy Ar ions (2 keV), followed directly by sputtering for 5 min with high energy Ar ions (4 keV). Commercial curve fitting software is used to highlight the peaks at 282 eV (highlighted in the upper two profiles).

Figure 6 shows the XPS spectra of both materials following this sputtering treatment and also the spectrum of the TiO_2 sample. The presence of the peak at 282 eV is clearly seen in the spectra of the two doped samples after sputtering and is absent in the case of the undoped TiO_2 material. Using these profiles it is possible to measure the concentration of dopant at the etched surface and it was found that in the case of the C-TiO_2 (He) sample, C was present at a concentration of 0.3 atom% while in the case of the C-TiO_2 (RCT) sample it was present at a level of 0.4 atom%. It should be recalled that this is the concentration of dopant C (as measured by comparing the intensity of the 282 eV peak with that of peaks relating to Ti and O) rather than the overall concentration of carbon on these materials (which was estimated above using TGA).

This conclusively shows that there is (as well as the graphitic and hydro-carbonaceous carbon-containing species discussed above), anionic dopant present within both samples, *i.e.* those prepared using a He heat treatment and a reduced temperature calcination of a titanium isopropoxide sol-gel derived powder

Figure 7

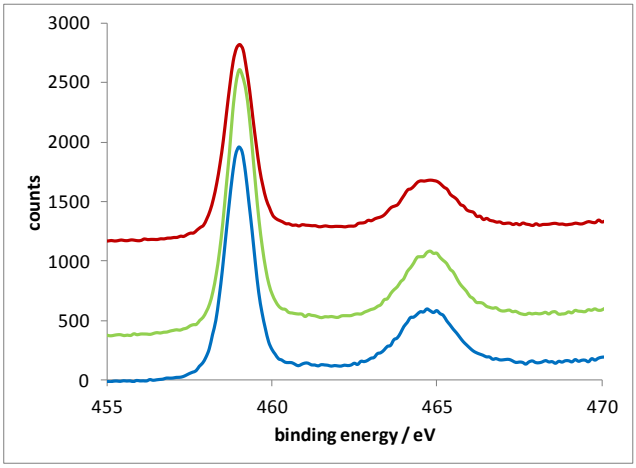

Figure 7. Displaced XPS spectra of the Ti 2p region (before sputtering) showing profiles relating to C-TiO_2 (RCT) (top profile), C-TiO_2 (He) (middle profile) and TiO_2 (lower profile). No features relating to Ti^{3+} are present.

Figure 7 shows the Ti 2p region of the XPS spectra of these materials before sputtering in an attempt to determine whether Ti^{3+} existed on the He-treated material. It should be noted that all materials showed evidence of Ti^{3+} following the sputtering treatment and it is known that such sputtering treatment does lead to reduction of Ti^{4+} [33].

This profile shows that the treatment of the catalyst precursor in Helium at 500 °C did not lead to the formation of Ti^{3+} sites in the surface layers. All the Ti 2p XPS profiles are identical and features relating to Ti^{3+} (which would be expected at ~457 eV) are absent. Recall the TGA measurements reported above show that the same material also showed evidence of the presence of deposited graphitic carbon. Therefore, in conclusion, it does not seem that there is an appreciable amount of Ti^{3+} on the surfaces of this material – and it seems that it was C(s) that was responsible for the extended absorption of light across the visible region of the spectrum seen in figures 2 and 3.

4.4. Photocatalytic oxidation of 4-chlorophenol

Figure 8

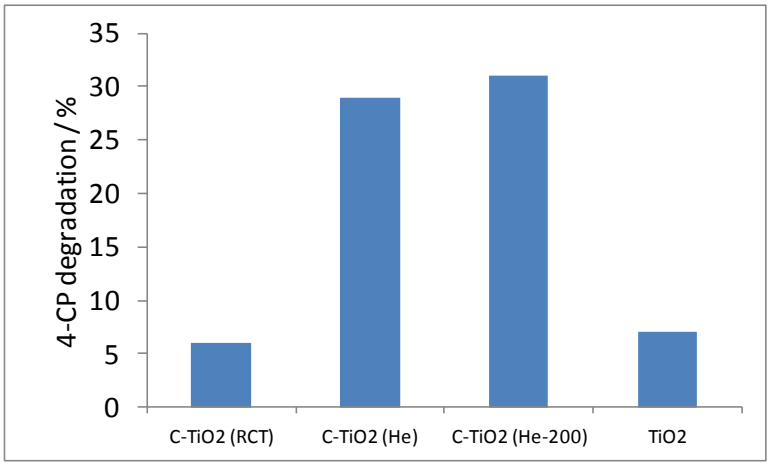

Figure 8. Photoactivity of several photocatalysts in the oxidation of 4-chlorophenol under visible-light-only conditions for 1h.

The initial (1h) photoactivity of the two catalysts were analysed in the oxidation of 4-chlorophenol under visible-light-only (λ > 410 nm) conditions and the results are shown in figure 8. The TiO_2 sample's activity was also monitored under these conditions. Analysis of figure 2 shows that all of these materials absorb a certain amount of light above 410 nm with the C-TiO_2 (He) sample absorbing the most followed by the C-TiO_2 (RCT) material and the TiO_2 (which has a small absorbance here).

After 1 h of reaction TOC measurements have shown that the C-TiO_2 (He) sample had degraded 29% of the 4-chlorophenol whereas C-TiO_2 (RCT) and TiO_2 were far less active (degrading 6% and 7% of the 4-chlorophenol respectively.

The low reactivity of the TiO_2 catalyst is to be expected given that the extent of light absorbance (and therefore reaction initiation) here is particularly low. Given the absorbance of light is important in initiating this reaction it is no surprise that the material with the highest absorbance under visible light conditions proved most active. However, it is clear that the other material that absorbs a significant amount of visible light (C-TiO_2 (RCT)) was in no way as active (decomposing only 6% of the organic material). XRD analysis has suggested that this material is significantly less crystalline than the C-TiO_2 (He) catalyst. This confirms that crystallininty is also an important metric for photocatalytic activity (since it allows for better electron / hole separation and therefore hinders electron hole recombination).

The final activity shown in figure 8 relates to that of a catalyst whose sol-gel derived precursor had been treated in O_2 at 200 °C for 2 minutes before being further treated to 500 °C in He. The UV Visible spectrum of this material is shown in figure 3(a). The low temperature oxidation removed a

certain amount of C from the sol-gel derived precursor while the high temperature excursion to 500 °C in He would be expected to promote crystallininty. This material was slightly more active than the C-TiO_2 (He) catalyst but significantly more active than the C-TiO_2 (RCT) material. Assuming that the treatment at 500 °C promotes crystallininty we can see that this has an important effect on reactivity.

Conclusions

The work reported above has shown that carbon remained on the surfaces of these two catalysts following their preparation (TGA / TPO) and that this carbon has affected the absorbance characteristics of the material (UV Visible spectroscopy). The nature of the carbon has been shown to include graphitic carbon in the case of the C-TiO_2 (He) catalyst and include hydro-carbonaceous material in the case of the C-TiO_2 (RCT) catalyst. The extent of graphitic carbon laydown could be tuned through the use of oxidation within the initial He heat treatments.

It has also been shown that the carbon has affected the crystal lattice of the TiO_2 (XRD). This result and the altered bandgaps of the materials determined using UV-visible spectroscopy suggest anionic doping of C atoms into the TiO_2 lattice. This is confirmed using XPS following a sputtering technique which removes surface carbon contamination and conclusively demonstrates the presence of a Ti-C dopant species alongside the graphitic or hydro-carbonaceous species.

The reactivity data has shown that extending the bandgap does impinge on the photo-oxidation activity of the materials under visible-light-only conditions but that it alone is not the only factor that contributes to reactivity and that the crystallininty of the material is also important. This crystallinity

is improved by high temperature treatments in He without losing any of the beneficial effects of the bandgap extending anionic C species.

Acknowledgements

We acknowledge and thank Science Foundation Ireland for their funding of this Strategic Research Cluster Programme (07/SRC/B1160) and our Industry Partners for their support of this Cluster. We specifically thank SSE Renewables for their support of E.M.N. We are also grateful to Anne-Katrin Prescher for assistance with TOC analysis. KRT acknowledges also the support received under the SFI-Airtricity-Stokes Professorship grant.

References

[1] Y. Li and J. Zhang, Laser & Photonics Reviews, 4 (2010) 517-528.

[2] A.J. Bard and M.A. Fox, Accounts of Chemical Research, 28 (1995) 141-145.

[3] R. Navarro, M. Sanchez-Sanchez, M. Alvarez-Galvan, F. Del Valle and J. Fierro, Energy and Environmental Science, 2 (2008) 35-54.

[4] N. Strataki, V. Bekiari, D.I. Kondarides and P. Lianos, Applied Catalysis B: Environmental, 77 (2007) 184-189.

[5] J.M. Herrmann, Catalysis Today, 53 (1999) 115-129..

[6] A. Patsoura, D.I. Kondarides and X.E. Verykios, Catalysis Today, 124 (2007) 94-102..

[7] J. Cunningham and P. Sedlak, Catalysis Today 29 (1996) 309-315

[8] M. Romero, J. Blanco, B. Sánchez, A. Vidal, S. Malato, A.I. Cardona and E. Garcia, Solar Energy, 66 (1999) 169-182.

[9] C.S. Turchi and D.F. Ollis, Journal of Catalysis, 122 (1990) 178-192.

[10] J. Yang, J. Dai, C. Chen and J. Zhao, Journal of Photochemistry and Photobiology A: Chemistry, 208 (2009) 66-77.

[11] C.A. Grimes, O.K. Varghese and S. Ranjan (Editors), Light, Water, Hydrogen: The Solar Generation of Hydrogen by Water Photoelectrolysis, Springer, 2008.

[12] A.L. Linsebigler, G. Lu and J.T. Yates Jr, Chemical Reviews, 95 (1995) 735-758.

[13] G.L. Chiarello, M.H. Aguirre and E. Selli, Journal of Catalysis, 273 (2010) 182-190.

[14] A. Zaleska, Recent Patents on Engineering, 2 (2008) 157-164.

[15] J. Choi, H. Park and M.R. Hoffmann, The Journal of Physical Chemistry C, 114 (2009) 783-792.

R. Asahi, T. Morikawa, T. Ohwaki, K. Aoki and Y. Taga, Science, 293 (2001) 269-271.

[16] D.M. Chen, Z.Y. Jiang, J.Q. Geng, Q. Wang and D. Yang, Industrial & Engineering Chemistry Research, 46 (2007) 2741-2746.

[17] H. Irie, Y. Watanabe and K. Hashimoto, Journal of Physical Chemistry B, 107 (2003) 5483-5486.

[18] S.U.M. Khan, M. Al-Shahry and W.B. Ingler, Science, 297 (2002) 2243-2245.

[19] Y.T. Lin, C.H. Weng, Y.H. Lin, C.C. Shiesh, F.Y. Chen, Separation and Purification Technology, 116 (2013) 114-123.

[20] Y. Park, W. Kim, H. Park, T. Tachikawa, T. Majima and W. Choi, Applied Catalysis B: Environmental, 91 (2009) 355-361.

[21] S. Sakthivel, M. Janczarek and H. Kisch, Journal of Physical Chemistry B, 108 (2004) 19384-19387.

[22] T. Tachikawa, S. Tojo, K. Kawai, M. Endo, M. Fujitsuka, T. Ohno, K. Nishijima, Z. Miyamoto and T. Majima, Journal of Physical Chemistry B, 108 (2004) 19299-19306.

[23] X.X. Yang, C.D. Cao, L. Erickson, K. Hohn, R. Maghirang and K. Klabunde, Journal of Catalysis, 260 (2008) 128-133.

[24] J. A. Sullivan, K.R. Thampi, E.M. Neville, M.J. Mattle, D. Loughrey, B. Rajesh, M. Rahman, J.M.D. MacElroy, Journal of Physical Chemistry C, (2012), 116, 16511−16521

[25] Y. Park, W. Kim, H. Park, T. Tachikawa, T. Majima and W. Choi, Applied Catalysis B: Environmental, 91 (2009) 355-361.

[26] X.X. Yang, C.D. Cao, L. Erickson, K. Hohn, R. Maghirang and K. Klabunde, Journal of Catalysis, 260 (2008) 128-133

[27] A.L. Patterson, Physical Review, 56 (1939) 978–982.

[28] R.A. Spurr and H. Myers, Analytical Chemistry, 29 (1957) 760-762.

[29] T J B Holland and S A T Redfern 61, (1997) Mineralogical Magazine 65-77.

[30] J.A. Sullivan and O. Keane. Catalysis Today, 114, (2006), 340-345.

[31] J.A. Sullivan, K.R. Thampi, E.M. Neville, J.M.D. MacElroy, Journal of Photochemistry and Photobiology A: Chemistry, 267, (2013), 17-24.

[32] J.A. Sullivan, J. Ziegler, K.R. Thampi, E.M. Neville, J.M.D. MacElroy, Applied Catalysis A:General, 470, (2014), 434-441.

[33] Hashimoto, S., Murata, A., Sakurada, T., Tanaka, A., Journal of Surface Analysis, 10, (2003), 12-15.